Kütahya Dumlupınar University
Institute of Graduate Studies

Journal of Scientific
Reports-A
E-ISSN: 2687-6167
Number 49, June 2022

RESEARCH ARTICLE

CONFINEMENT EFFECTS on the TRANSPORT PROPERTIES of ROOM TEMPERATURE IONIC LIQUID BASED ELECTROLYTES in SUPERCAPACITORS

Betul URALCAN*

*Bogazici University, Department of Chemical Engineering and Polymer Research Center, betul.uralcan@boun.edu.tr, ORCID: 0000-0002-0669-8441

Receive Date:26.05.2022 *Accepted Date: 18.06.2022*

ABSTRACT

The study of transport properties in supercapacitors is important for optimizing their power density. Properties that control charging kinetics in supercapacitors include ion self-diffusion coefficients and ionic conductivity which are significantly different at electrode/electrolyte interfaces compared to their bulk counterparts. Here, we use molecular dynamics simulations to elucidate the effect of electrolyte composition and confinement on ion self-diffusion coefficients and ionic conductivity in mixtures of room temperature ionic liquids with organic solvents. Our results reveal that ion diffusion significantly slows down at the electrode/electrolyte interface compared to the bulk. In particular, diffusion coefficients in the dilute regime are found to be several orders of magnitude smaller than their bulk counterparts. This effect is more pronounced when a potential difference is applied between the electrodes. We show that the ionic conductivity of the electrolytes also significantly diminishes due to confinement effects manifested by the decrease in the coordination numbers of ions. Our findings depict that electrolyte composition also plays an important role in ion dynamics: Introduction of an organic solvent to a concentrated ionic solution significantly increases both bulk and interfacial diffusion coefficients while it leads to a maximum in ionic conductivity at intermediate dilution levels. These results reveal that optimizing the solvent content of an ionic liquid-based electrolyte can potentially boost the power density of supercapacitors.

Keywords: *energy storage, supercapacitors, molecular dynamics, diffusivity, conductivity*

1. INTRODUCTION

Supercapacitors are energy storage devices that can deliver bursts of energy at high power densities through storing charges at an electrode/electrolyte interface [1–3]. Despite their lower energy densities compared to conventional electrochemical energy storage devices such as batteries, supercapacitors are already employed in high power applications such as blade angle control systems of wind turbines, battery-assist and regenerative power systems of electric/hybrid cars, and engine starts for construction and industrial equipment [4].

The performance of a supercapacitor is based on two principal metrics: energy density (E) in units (Wh/kg or Wh/cm^3) and power density (P) in units (W/kg or W/cm^3) [5, 6]. Energy density dictates the ability of a device to store energy per unit mass or volume, and is given by

JSR A
Journal of Scientific Reports

$$\boldsymbol{E = \frac{1}{2} C U^2} \quad (1)$$

where *C* is the capacitance and *U* is the operating voltage.

In contrast to batteries that involve faradaic reactions, supercapacitors store energy through physical adsorption of ions as a response to an applied potential difference, where electrode charge is balanced by the accumulation of opposite ionic charges at the interface [7, 8]. The physical charge storage mechanism through ion adsorption and desorption facilitates fast charge and discharge kinetics in supercapacitors, and power density describes the charge/discharge rates

$$\boldsymbol{P = \frac{U^2}{ESR}} \quad (2)$$

where *ESR* is the equivalent series resistance of the device. *U* and *ESR* strongly depend on both electrode and electrolyte properties. Consequently, on the electrode side, research on improving power density is focused on synthesizing electrochemically stable (for higher *U*) and electrically conductive (for smaller *ESR*) carbon-based materials with large surface area and optimized pore structure [8]. Meanwhile, on the electrolyte side, the ultimate goal is to deliver electrolyte materials with high electrochemical stability and ionic conductivity. Consequently, optimizing power density in supercapacitors requires elucidating how ion diffusion at an electrode/electrolyte interface is affected from electrolyte composition [9–11].

In supercapacitors, dilute electrolytes comprised of salts dissolved in organic solvents (e.g., tetraethylammonium tetrafluoroborate in acetonitrile) are commonly used as electrolytes [12]. These electrolytes offer relatively high electrochemical stability at operating voltages around ~2.5 V and high ionic conductivities at room temperature (up to ~60 mS/cm) [13]. Aqueous electrolytes provide even higher conductivities (exceeding 100 mS/cm) and are cost effective, yet, unless cost is the primary factor, they can not compete with organic electrolytes as their electrochemical stability window is limited to ~1 V [12, 13]. Room temperature ionic liquids (RTILs) emerge as electrochemically stable electrolytes (~4 V) that deliver high energy densities (Equation 1) [14]. However, the enhanced energy density of RTIL-based supercapacitors comes at a cost, namely low power density associated with the diminished ionic conductivity and slow ion transport at room temperature. Consequently, elucidating the charge storage mechanisms and kinetics of supercapacitors is critical in optimizing transport properties in supercapacitors to boost power performance [2, 8, 15–19].

While a wide literature exists on bulk electrolyte properties, interfacial transport properties of RTIL-based electrolytes at charged electrode/electrolyte interfaces remain to be explored. Previous studies have shown that diffusion properties of confined liquids are significantly different from their bulk counterparts [20–22]. In particular, computational studies have shown anomalies in the diffusion coefficients of hard sphere fluids, water, oxygen and alkanes under confinement[23–25] that behave significantly different than they do in bulk. These findings have been of interest in applications that include ion transport through desalination membranes and drug delivery [23]. However, kinetics of concentrated ionic solutions under confinement and near charged interfaces remain to be explored. For this purpose, experimental techniques including NMR spectroscopy [26], scattering approaches [27], electrochemical quartz crystal microbalance [28] and IR spectroscopy [29] are used to show that charging properties of supercapacitors are sensitive to electrode and electrolyte materials

JSR A
Journal of Scientific Reports

combinations. Nevertheless, experiments lack the spatiotemporal resolution to fully elucidate charge storage mechanisms and kinetics at the atomistic level. Here, molecular modeling becomes significant in studying the effect of electrolyte properties on charging kinetics.

In this work, we study the relationship between solvation, electrolyte diffusion and ionic conductivity at an electrode/electrolyte interface. The rest of this paper is organized as follows. First, we describe the simulation system and introduce the model parameters that we use to set up the simulation systems. Then, we establish connections between the local structuring of confined electrolytes and the anomalous behavior of self-diffusivities. We show confinement slows down ion transport, and this effect is enhanced near charged surfaces. We then depict how a maximum in ionic conductivity emerges due to the presence of competing forces associated with solvation. To the best of our knowledge, self-diffusion and ionic conductivity in RTIL-based electrolytes under confinement has not been studied before. Finally, we provide concluding remarks and potential future directions.

2. COMPUTATIONAL DETAILS

2.1. Simulation Setup for Bulk Electrolyte

Bulk electrolytes are comprised of molecular simulation models of the ionic liquid 1-butyl-3-methylimidazolium hexafluorophosphate ([$BMIM^+$][PF_6^-]) [30] and organic solvent acetonitrile (ACN) [31]. These simulations are used to compute the bulk density of the electrolytes used in Section 2.2. In particular, seven different electrolytes are prepared: pure [$BMIM^+$][PF_6^-] and its corresponding ion fraction (ρ) = 0.03, 0.12, 0.26, 0.36, 0.47 and 0.67 solutions with ACN. For all electrolyte species, parameters of the coarse-grained models with site-site Lennard–Jones and Coulombic interactions are given in Table 1. The cross-parameters are computed using the standard Lorentz-Berthelot combination mixing rules. The solvent and cation are kept rigid using the SHAKE algorithm for computational efficiency [32]. The simulations are conducted in a cubic box. The isobaric-isothermal ensemble simulations at 5 atm and 400 K are done with the LAMMPS software [33] using the Nosé–Hoover thermostat and barostat. For the Lennard-Jones interactions, a 16 Å cut-off was used which corresponds to the half of the simulation box length. The particle-particle particle-mesh solver is employed for Coulombic interactions [34]. Equilibration simulations were run for 5 ns. Additional 5 ns production runs are carried out and the trajectories are used to compute bulk densities.

Table 1. Force field parameters for PF_6^- (A) [30], $BMIM^+$ (C1, C2, C3) [30], acetonitrile (ME, CA, N) [31] and electrodes (C) [35].

Particle ID	**A**	**C1**	**C2**	**C3**	**ME**	**CA**	**N**	**C**
***MW* (g/mol)**	144.96	67.07	15.04	57.12	15.04	12.01	14.01	12.01
***q* (e)**	-0.78	0.4374	0.1578	0.1848	0.269	0.129	-0.398	-
σ (Å)	5.06	4.38	3.41	5.04	3.60	3.40	3.30	3.37
ϵ (kcal/mol)	1.126	0.612	0.086	0.437	0.38002	0.10038	0.10038	0.055

2.2. Simulation Setup for Supercapacitor Systems

Supercapacitor models are comprised of the electrolytes with ρ values given in Section 2.1, confined by flat electrodes representing graphene sheets modelled as three layers of carbon atoms arranged in a honeycomb lattice. Electrode model parameters are adopted from Cole et al. [35] and reported in

JSR A
Journal of Scientific Reports

Table 1. The cross parameters between electrodes and electrolyte molecules are computed using the Lorentz-Berthelot rules. The force-field combination in Table 1 has been previously used in modelling ionic solutions both in bulk and under confinement, and has shown good agreement with experiments [8, 36–39]. İsochoric-isothermal ensemble simulations are conducted using the Nosé–Hoover thermostat. Periodic boundary conditions are employed in the directions parallel to the electrode surface, while boundaries are fixed in the direction normal to electrodes. Simulation systems are set up so that the bulk electrolyte mass densities (computed in Section 2.1) are reproduced in the bulk electrolyte region (Ωb) of the supercapacitor systems (Figure 1). This is achieved by tuning the location of the electrodes in the z-direction and conducting 0.5 ns equilibration runs until the target density is reached. Once the target density is reached, systems are further equilibrated for 2 ns, followed by 10 ns production runs at zero charge. The production data is used to compute transport and structural properties of the systems with uncharged electrodes. Afterwards, electrodes are charged to maintain a 1.5 V potential difference between the electrodes. 1.5 V corresponds to potential difference limit under which an RTIL-based electrolyte in an organic solvent remains electrochemically stable [12, 14]. 10 ns simulations of the charged systems are carried out for equilibration, followed by additional 10 ns production runs at constant charge. The equilibration simulations are run long enough to maintain the equilibrium charge ordering at the electrode/electrolyte interface. The production runs are extended until the convergence of kinetic properties are ensured (see Section 2.3 for details.)

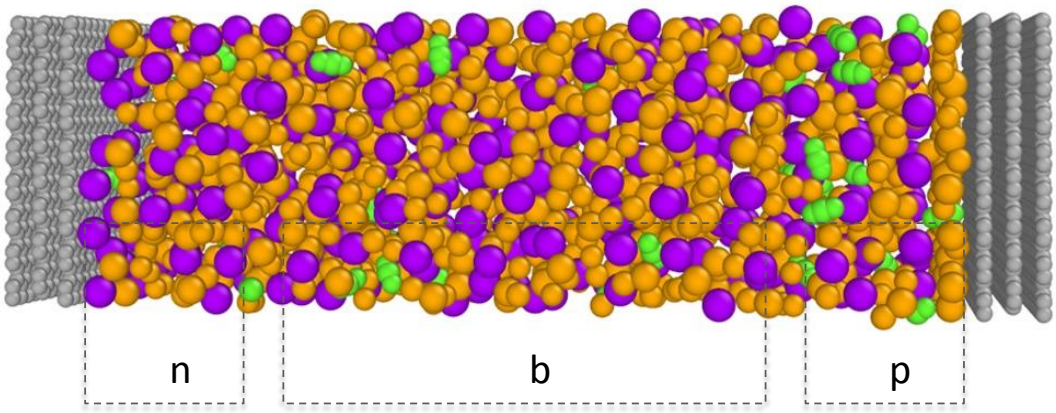

Figure 1. Simulated supercapacitor consists of a room temperature ionic liquid (orange for [$BMIM^+$] and purple for [PF_6^-]) - organic solvent (green for ACN) electrolyte sandwiched between two electrodes modelled as three layers of hexagonal carbon lattices. Three regions are defined within the system, namely the bulk electrolyte (Ωb) and interfacial regions (Ωn and Ωp). The electrolyte has ρ = 0.67.

2.3. Self-diffusion Coefficient and Conductivity Calculations

Self-diffusion is a measure of the average displacement of a molecule from its initial position due to thermal molecular motion. It describes how fast a material can diffuse through a medium. Self-diffusion coefficients for the bulk electrolytes are computed using the Einstein relation where the mean-square displacement (MSD) of molecules is computed as a function of time and the linear regime of the MSD profile is used to compute the self-diffusion coefficient D_i

JSR A
Journal of Scientific Reports

$$D_i = \lim_{t\to\infty} \frac{\langle (r_i(t) - r_i(0))^2 \rangle}{6t} \quad (3)$$

with $r_i(t)$ as the instantenous center of mass of ion type *i* and <...> as the average over all type *i* ions in the ensemble. Diffusion coefficients are computed from the production run trajectories block-averaged in 1 ns long sections. The position-dependent self-diffusion coefficients are computed for the ions in bulk (Ωb) and at the electrode/electrolyte interface (Ωn and Ωp) following Zhang et al. [40]. Since ions can penetrate in and move out of the interface during a simulation, only the ions that remain in the defined regions during 1 ns blocks are considered to compute D_i. Electrolyte ionic conductivity (κ) is calculated using the Nernst-Einstein equation via the weighted sum of the ion self-diffusion coefficients.

3. RESULTS and DISCUSSION

Diffusion in confined liquids differ from diffusion in bulk. In particular, diffusion near walls is influenced by liquid-solid interactions which results in density fluctuations at the interface [23]. In order to compute the bulk and interfacial ion self-diffusion coefficients for the simulation system presented in Figure 1, three regions are defined within the system, namely the bulk electrolyte 25 Å away from the electrode surface (Ωb) and interfacial regions encompassing the first two solvation layers of the ions near the electrode (Ωn and Ωp).

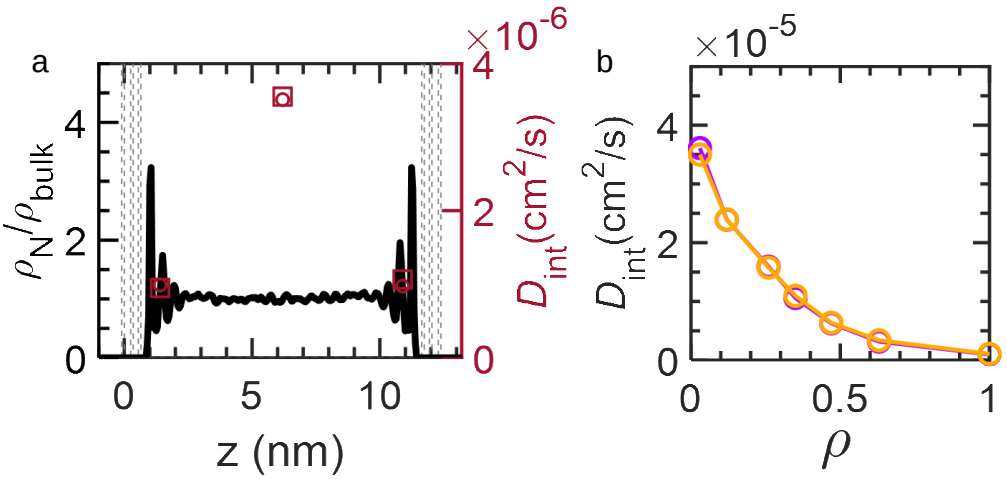

Figure 2. (a) Position dependent number density profile of the electrolyte parallel to the basal plane of the electrodes (*left axis*) and spatial evolution of the anion (circles) and cation (squares) diffusion coefficients for Ωn, Ωp and Ωb (*right axis*) for the system with ρ = 0.67, (b) Self-diffusion coefficients of cation (orange) and anion (purple) as a function of ion fraction near uncharged electrodes.

Figure 2a shows the number density profile of the electrolyte confined between the uncharged electrodes (ρ_N) normalized by the bulk number density (ρ_{bulk}) in Figure 1. Near the electrode surfaces (Ωn and Ωp), there is a non-uniform particle distribution. In particular, electrolyte that is close to the electrodes shows large density fluctuations due to strong electrode/electrolyte interactions that restrict

JSR A
Journal of Scientific Reports

kinetics. Meanwhile, at the center of the pore (Ωb), the confinement effect vanishes. Hence, while the self-diffusion coefficients in the bulk are on the order of $4.5*10^{-6}$ cm^2/s, near the electrodes they are only around $1.2*10^{-6}$ cm^2/s as confinement slows down the dynamics (Figure 2a). The difference between

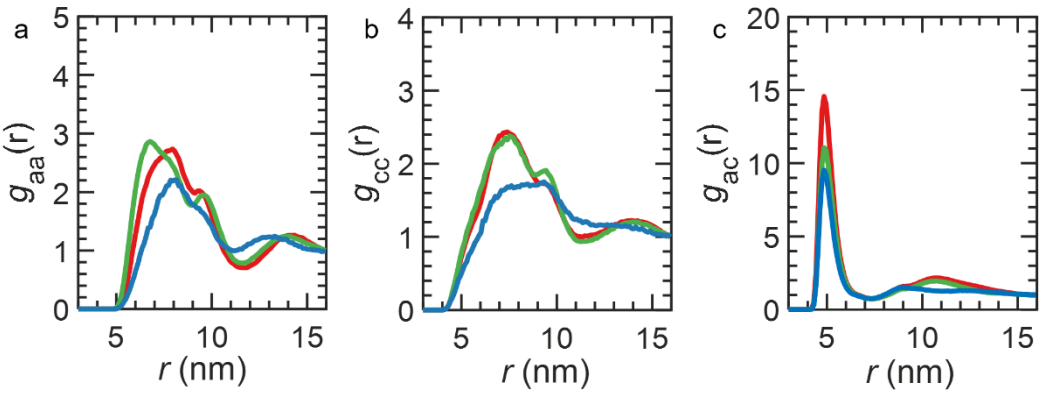

Figure 3. Composition dependence of pairwise radial distribution profiles for (a) anion-anion, (b) cation-cation, and (c) anion-cation interactions. Blue, green and red represent ρ = 0.26, 0.67 and 1.0, respectively.

the interfacial and bulk diffusion coefficients entails a pure confinement effect: In particular, the structuring of the ions within the first two adsorbed layers near the electrodes depicted by the peaks of the number density profile (Figure 2a) slows down ion kinetics.

The question that is next to be addressed is how this surface effect depends on the dilution of the ionic liquid by a solvent. In particular, Figure 2b shows the diffusion coefficients near the uncharged electrode surfaces when [$BMIM^+$] [PF_6^-] is diluted with the organic solvent ACN. At the interface, introduction of the solvent significantly increases the self-diff usion coefficients for the anion and the cation (Figure 2b). In particular, decreasing the ion fraction from ρ = 1 to ρ = 0.03 enhances the ion self-diff usion coefficients by more than an order of magnitude.

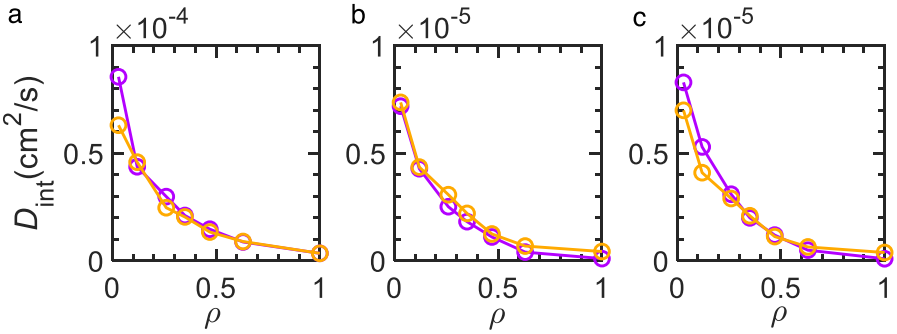

Figure 4. Composition dependence of self-diffusion coefficients for anion (purple), cation (orange) (a) in the bulk, (b) near the negative electrode, and c) near the positive electrode.

JSR A
Journal of Scientific Reports

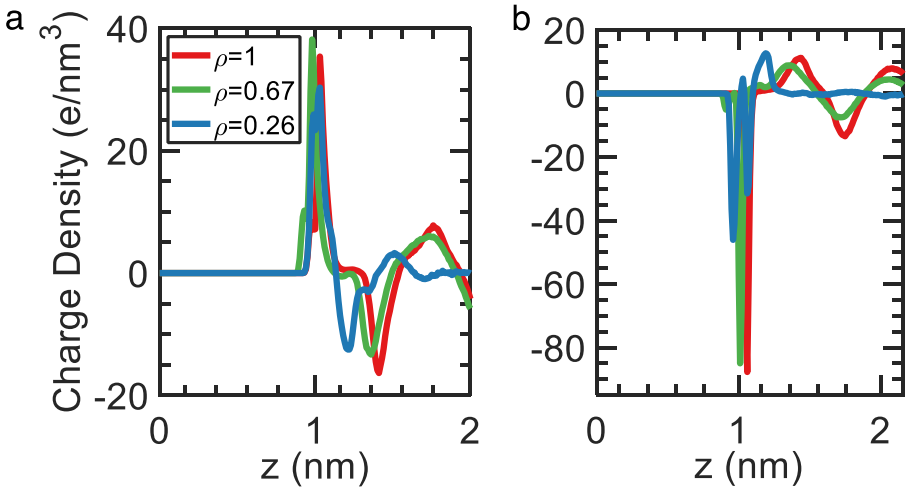

Figure 5. Charge density profile as a function of distance from the (a) negative and (b) positive electrode surface for ρ = 0.26 (blue), 0.67 (green) and 1.0 (red).

Interestingly, Figure 2 also shows that the anion and cation self-diffusion coefficients are significantly close to each other throughout the entire concentration regime, indicating that cations and anions remain strongly correlated even when they are solvated, indicated by Figure 3c with the pronounced first peaks of the anion-cation radial distribution profiles normalized by the number in bulk (i.e., when the molecules are further apart and uncorrelated). The pairwise radial distribution functions (RDFs) suggest a preferential interaction should result in a higher peak in the radial distribution functions: In Figure 3, the first peak height is the highest for anion-cation interactions. This indicates that anions are preferentially located around cations in the electrolyte. The broader and lower first peaks in the anion-anion ($g_{aa}(r)$) and cation-cation ($g_{cc}(r)$) profiles indicate that co-ions interact weakly. The RDFs of the anion around the cation indicate the first peak is near 5 Å. The peak distance is not correlated with solvent composition as the peak does not shift with dilution (Figure 3c), but the peak height decreases with increasing solvent concentration. This indicates that cation-anion correlations decrease with solvation. Figure 3a-b show that, although the effect of solvation is not significant when the electrolyte concentration changes from ρ = 1 to ρ = 0.67, when the electrolyte is diluted to ρ = 0.26, the first peak heights of $g_{aa}(r)$ and $g_{cc}(r)$ decrease with dilution. Furthermore, the first peak shifts to larger distances when the pure ionic liquid is diluted from ρ = 1 to ρ = 0.26. This indicates that correlations between ions of the same charge weaken with solvation and ion pairs become more separated improving diffusion kinetics.

We next investigate the diffusion kinetics of the electrolytes near charged electrode surfaces under equilibrium. The difference between diffusion coefficients in the bulk and at the interface further increases when the system is charged, i.e., a potential difference is applied between the electrodes. Figure 4 shows the ion self-diffusion coefficients in the bulk and near the positively and negatively charged electrodes as a function of ionic liquid fraction. Compared to the bulk (Figure 4a) and noncharged interfaces (Figure 2b), confinement at a charged interface significantly slows down ion

JSR A
Journal of Scientific Reports

kinetics (Figure 4b-c). The charge density profiles in Figure 5 sheds light onto this behavior. Near the charged electrodes, the electrolyte is highly charge-ordered as shown in Figure 5. This is due to the

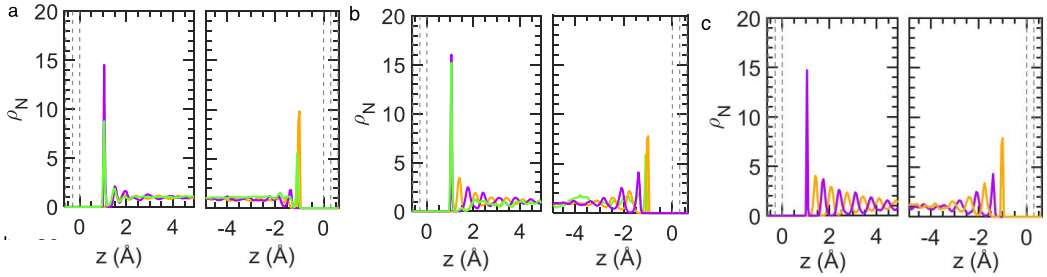

Figure 6. Number density profiles for anion (purple), cation (orange) and solvent (green) molecules as a function of distance from the positive (left) and negative (right) electrodes for (a) ρ = 0.26, (b) ρ = 0.67 and (c) ρ = 1.0.

layering of the ions (Figure 6) to screen the electrode charges. In particular, since the electric field stabilizes the ions in the direction normal the basal plane of the electrodes, confined electrolytes at charged surfaces have an order of magnitude slower kinetics than their bulk counterparts.

When the electrolyte near a charged surface is diluted, charge ordering weakens, and ions can move more freely enhancing diffusion kinetics. This is shown by the dampening of the charge density profile peaks with dilution in Figure 5. When the electrolyte is pure ionic liquid, charge ordering at the interface is highly structured as anions and cations are significantly correlated and this leads to overscreening and crowding effects [41–43]. When the electrolyte is diluted, anion-cation interactions weaken hence the peak heights of the charge density profile dampens leading to improved kinetics depicted by the diffusion coefficient profiles in Figure 4b-c.

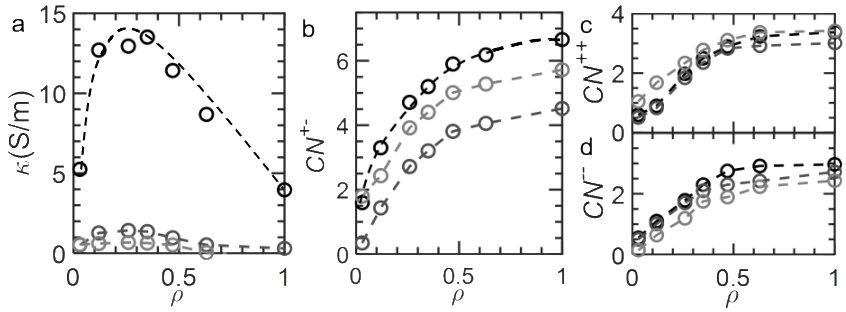

Figure 7. Composition dependence of ion dynamics in the electrolyte. (a) Ionic conductivity (κ), (b) cation-anion coordination number (CN^{+-}), (c) cation-cation coordination number (CN^{++}), (d) anion-anion coordination number (CN^{--}) as a function of electrolyte ion fraction. Black, dark gray and light gray circles represent the bulk electrolyte and the electrolye near the negative and positive electrodes, respectively. Lines are guides to the eye.

JSR A
Journal of Scientific Reports

The ionic conductivity profiles of the electrolyte in bulk and near charged surfaces as a function of ion content (Figure 7a) shows how ionic conductivity is affected from dilution. The electrolyte composition dependence of κ in bulk (black circles) is in qualitative agreement with experimental measurements [44-45]. In the dilute regime, solvation decreases ionic conductivity. This is attributable to the decrease in the number of free ions in bulk with solvation. To illustrate this point, Figure 7b-d shows how the coordination number of ions around each other (CN^{+-} for anions around cations and CN^{++} (CN^{--}) for cations around cations (anions around anions)) changes with concentration. Both in bulk and at the interface, solvation decreases the number of ions around each other. In particular, bulk CN^{+-} decreases from 6.8 to 1.6 as the electrolyte is diluted down to ρ = 0.03. In agreement with the Nernst-Einstein theory, the effect of decreasing free ions becomes dominant at high dilution, leading to a drop in ionic conductivity. In the concentrated regime, on the other hand, the dominant factor is solvent's ability to enhance ion mobility, thus solvation improves conductivity by increasing ion diffusivities. Consequently, these two competing forces, namely the trade-off between decreasing ion content with solvation dominant in the dilute regime and improved diffusivity with dilution dominant in the concentrated regime, results in a maximum in conductivity at intermediate dilution levels. As a result of this competition, for [$BMIM^+$][PF_6^-] in ACN, the maximum in ionic conductivity is observed near ρ = 0.26 at 13.9 S/m. We note that a similar nonmonotonic behavior is also observed near the charged and uncharged interfaces albeit with nearly an order of magnitude smaller ionic conductivity values (Figure 7a). *CN*s are slightly smaller at interfacial regions Ωn and Ωp due to the presence of carbon electrode/electrolyte interactions. Yet, qualitatively similar *CN* profiles are obtained near charged and uncharged surfaces as a function of solvation (Figure 7b-d). While total CN values (CN^{++} + CN^{--} + CN^{+-}) are similar in magnitude both near charged and uncharged electrodes, near the charged surfaces counter-ions are replaced by co-ions as seen from the decrease in CN^{+-} and increase in CN^{++} and CN^{--} profiles upon charging (Figure 7c-d). This is reflected in the small decrease in interfacial conductivity upon charging due to the strong charge ordering of the ions, as reflected in Figure 7a.

4. CONCLUSION

Transport properties of room temperature ionic liquids and their solutions in ACN are investigated using molecular dynamics simulations. The simulations reveal that ion kinetics under confinement significantly differ from the kinetics of their bulk counterparts. Bulk simulations indicate that the introduction of the solvent enhances ion self-diffusion coefficients while weakening the correlations between ions. The same solvation effect is also observed at the charged interfaces, but the magnitude of the diffusion coefficients at the interface are significantly lower than the ones in bulk. This is attributable to the charge ordering at the interface due to the layering of the ions to balance the electrode charges. Our results show introduction of the solvent drastically improves ion kinetics at the interface. The simulations also reveal that dilution imposes two competing effects on conductivity both in bulk and at the interface. At the concentrated regime, conductivity is improved with dilution as solvent dampens ion correlations and charge ordering. Meanwhile, in the dilute regime, diluting the electrolyte further decreases the conductivity due to decreasing free ion concentration. This competition results in a conductivity maximum both at the interface and in bulk. Our work demonstrates the kinetics of supercapacitors can be improved by tailoring electrolyte properties with the support of molecular modelling to facilitate supercapacitor design with improved power density. Extending the findings of this work to supercapacitor models with more complex electrode structures can facilitate designing supercapacitors with improved energy storage performance.

ACKNOWLEDGEMENTS

This work was supported by The Scientific and Technological Research Council of Turkey (TUBITAK) under BIDEB 2232-A (Project Number T118C220) and Bogazici University Research Fund (Project Number 17841).

REFERENCES

[1] Béguin, F., Presser, V., Balducci, A., Frackowiak, E., (2014), Carbons and Electrolytes for Advanced Supercapacitors. Advanced Materials, 26, 2219-2251.

[2] Simon, P., Gogotsi, Y., (2013), Capacitive Energy Storage in Nanostructured Carbon–Electrolyte Systems. Accounts of Chemical Research, 46, 1094-1103.

[3] Stoller, M. D., Park, S., Zhu, Y., An, J., Ruoff, R. S., (2008), Graphene-Based Ultracapacitors. Nano Letters, 8(10), 3498-3502.

[4] Wong, S. I., Sunarso, J., Wong, B. T., Lin, H., Yu, A., Jia, B., (2018), Towards enhanced energy density of graphene-based supercapacitors: Current status, approaches, and future directions. Journal of Power Sources, 396, 182‑206.

[5] Aslyamov, T., Sinkov, K., Akhatov, I., (2022), Relation between Charging Times and Storage Properties of Nanoporous Supercapacitors. Nanomaterials, 12, 587.

[6] Liu, T., Zhang, F., Song, Y., Li, Y., (2017), Revitalizing carbon supercapacitor electrodes with hierarchical porous structures. Journal of Materials Chemistry A, 5, 17705-17733.

[7] Péan, C., Merlet, C., Rotenberg, B., Madden, P. A., Taberna, P.-L., Daffos, B., Salanne, M., Simon, P., (2014), On the Dynamics of Charging in Nanoporous Carbon-Based Supercapacitors. ACS Nano, 8(2), 1576-1583.

[8] Pean, C., Rotenberg, B., Simon, P., Salanne, M., (2016), Understanding the different (dis)charging steps of supercapacitors: influence of potential and solvation. Electrochimica Acta, 206, 504-512.

[9] Uralcan, B., Aksay, I. A., Debenedetti, P. G., Limmer, D. T., (2016), Concentration Fluctuations and Capacitive Response in Dense Ionic Solutions. The Journal of Physical Chemistry Letters, 7(13), 2333-2338.

[10] Bozym, D. J., Uralcan, B., Limmer, D. T., Pope, M. A., Szamreta, N. J., Debenedetti, P. G., Aksay, I. A., (2015), Anomalous Capacitance Maximum of the Glassy Carbon-Ionic Liquid Interface through Dilution with Organic Solvents. The Journal of Physical Chemistry Letters, 6(13), 2644-2648.

JSR A
Journal of Scientific Reports

[11] Uralcan, B., Uralcan, I. B., (2022)., Origin of Enhanced Performance in Nanoporous Electrical Double Layer Capacitors: Insights on Micropore Structure and Electrolyte Composition from Molecular Simulations. ACS Applied Materials & Interfaces, 14(14), 16800-16808.

[12] Pal, B., Yang, S., Ramesh, S., Thangadurai, V., & Jose, R., (2019), Electrolyte selection for supercapacitive devices: a critical review. Nanoscale Advances, 1(10), 3807-3835.

[13] Cheng, Z., Yida D., Wenbin, H., Daoming, S., Jinli, Q., Jiujun, Z., (2016), Electrolytes for Electrochemical Supercapacitors. Routledge & CRC Press.

[14] Yu, L., Chen, G. Z., (2019), Ionic Liquid-Based Electrolytes for Supercapacitor and Supercapattery. Frontiers in Chemistry, 7.

[15] Lian, Z., Chao, H., Wang, Z.-G., (2021), Effects of Confinement and Ion Adsorption in Ionic Liquid Supercapacitors with Nanoporous Electrodes. ACS Nano, 15(7), 11724-11733.

[16] Lin, R., Huang, P., Ségalini, J., Largeot, C., Taberna, P. L., Chmiola, J., Gogotsi, Y., Simon, P., (2009), Solvent effect on the ion adsorption from ionic liquid electrolyte into sub-nanometer carbon pores. Electrochimica Acta, 54(27), 7025-7032.

[17] Feng, G., Qiao, R., Huang, J., Sumpter, B. G., Meunier, V., (2010), Ion Distribution in Electrified Micropores and Its Role in the Anomalous Enhancement of Capacitance. ACS Nano, 4(4), 2382-2390.

[18] Oyarzun, D. I., Zhan, C., Hawks, S. A., Cerón, M. R., Kuo, H. A., Loeb, C. K., Aydın, F., Pham, T. A., Stadermann, M., Campbell, P. G., (2021), Unraveling the Ion Adsorption Kinetics in Microporous Carbon Electrodes: A Multiscale Quantum-Continuum Simulation and Experimental Approach. ACS Applied Materials & Interfaces, 13(20), 23567-23574.

[19] Lahrar, E. H., Deroche, I., Matei Ghimbeu, C., Simon, P., Merlet, C., (2021), Simulations of Ionic Liquids Confined in Surface-Functionalized Nanoporous Carbons: Implications for Energy Storage. ACS Applied Nano Materials, 4(4), 4007-4015.

[20] Walton, J. P. R. B., Quirke, N., (1989), Capillary Condensation: A Molecular Simulation Study. Molecular Simulation, 2(4‐6), 361-391.

[21] Mu, R., Malhotra, M. V., (1991), Effects of surface and physical confinement on the phase transitions of cyclohexane in porous silica. Physical Review. B, Condensed Matter, 44(9), 4296-4303.

[22] Gelb, L. D., Gubbins, K. E., Radhakrishnan, R., Sliwinska-Bartkowiak, M., (1999), Phase separation in confined systems. Reports on Progress in Physics, 62(12), 1573-1659.

[23] Spera, M. B. M., Franco, L. F. M., (2020), Surface and confinement effects on the self-diffusion coefficients for methane-ethane mixtures within calcite nanopores. Fluid Phase Equilibria, 522, 112740.

[24] Wang, G. J., & Hadjiconstantinou, N. G. (2018). Layered Fluid Structure and Anomalous Diffusion under Nanoconfinement. Langmuir, 34(23), 6976-6982.

[25] Leoni, F., Calero, C., Franzese, G., (2021), Nanoconfined Fluids: Uniqueness of Water Compared to Other Liquids. ACS Nano, 15(12), 19864-19876.

[26] Griffin, J. M., Forse, A. C., Wang, H., Trease, N. M., Taberna, P.-L., Simon, P., Grey, C. P., (2015), Ion counting in supercapacitor electrodes using NMR spectroscopy. Faraday Discussions, 176(0), 49-68.

[27] Boukhalfa, S., He, L., Melnichenko, Y. B., Yushin, G., (2013), Small-angle neutron scattering for in situ probing of ion adsorption inside micropores. Angewandte Chemie (International Ed. in English), 52(17), 4618-4622.

[28] Levi, M. D., Salitra, G., Levy, N., Aurbach, D., Maier, J., (2009), Application of a quartz-crystal microbalance to measure ionic fluxes in microporous carbons for energy storage. Nature Materials, 8(11), 872-875.

[29] Richey, F. W., Dyatkin, B., Gogotsi, Y., Elabd, Y. A., (2013), Ion Dynamics in Porous Carbon Electrodes in Supercapacitors Using in Situ Infrared Spectroelectrochemistry. Journal of the American Chemical Society, 135(34), 12818-12826.

[30] Roy, D., Patel, N., Conte, S., Maroncelli, M., (2010), Dynamics in an Idealized Ionic Liquid Model. The Journal of Physical Chemistry B, 114(25), 8410-8424.

[31] Edwards, D. M. F., Madden, P. A., McDonald, I. R., (1984), A computer simulation study of the dielectric properties of a model of methyl cyanide. Molecular Physics, 51(5), 1141-1161.

[32] Ryckaert, J.-P., Ciccotti, G., Berendsen, H. J. C., (1977), Numerical Integration of the Cartesian Equations of Motion of a System with Constraints: Molecular Dynamics of n-Alkanes. Journal of Computational Physics, 23, 327-341.

[33] Thompson, A. P., Aktulga, H. M., Berger, R., Bolintineanu, D. S., Brown, W. M., Crozier, P. S., Veld, P J., Kohlmeyer, A., Moore, S. G., Nguyen, T. D., Shan, R., Stevens, M. J., Tranchida, J., Trott, C., Plimpton, S.J., (2022), LAMMPS - a flexible simulation tool for particle-based materials modeling at the atomic, meso, and continuum scales. Computer Physics Communications, 271, 108171.

[34] Hockney, R. W., Eastwood, J. W., (2021), Computer Simulation Using Particles. CRC Press.

[35] Cole, M. W., Klein, J. R., (1983), The interaction between noble gases and the basal plane surface of graphite. Surface Science, 124(2‐3), 547-554.

[36] Merlet, C., Rotenberg, B., Madden, P. A., Salanne, M., (2013), Computer simulations of ionic liquids at electrochemical interfaces. Physical Chemistry Chemical Physics, 15(38), 15781-15792.

[37] Merlet, C., Péan, C., Rotenberg, B., Madden, P. A., Daffos, B., Taberna, P.-L., Simon, P., Salanne, M., (2013), Highly confined ions store charge more efficiently in supercapacitors. Nature Communications, 4, 2701.

[38] Merlet, C., Péan, C., Rotenberg, B., Madden, P. A., Simon, P., Salanne, M., (2013), Simulating Supercapacitors: Can We Model Electrodes As Constant Charge Surfaces? The Journal of Physical Chemistry Letters, 4(2), 264-268.

[39] Péan, C., Merlet, C., Rotenberg, B., Madden, P. A., Taberna, P.-L., Daffos, B., … Simon, P., (2014), On the Dynamics of Charging in Nanoporous Carbon-Based Supercapacitors. ACS Nano, 8(2), 1576-1583.

[40] Zhang, Y., Cummings, P. T., (2019), Effects of Solvent Concentration on the Performance of Ionic-Liquid/Carbon Supercapacitors. ACS Applied Materials & Interfaces, 11(45), 42680-42689.

[41] Kondrat, S., Kornyshev, A., (2010), Superionic state in double-layer capacitors with nanoporous electrodes. Journal of Physics: Condensed Matter, 23(2), 022201.

[42] Kornyshev, A. A., (2007), Double-Layer in Ionic Liquids: Paradigm Change? The Journal of Physical Chemistry B, 111(20), 5545-5557.

[43] Bazant, M. Z., Storey, B. D., Kornyshev, A. A., (2011), Double layer in ionic liquids: overscreening versus crowding. Physical Review Letters, 106(4), 046102.

[44] Zhu, A., Wang, J., Han, L., Fan, M., (2009), Measurements and correlation of viscosities and conductivities for the mixtures of imidazolium ionic liquids with molecular solutes. Chemical Engineering Journal, 147(1), 27-35.

[45] Roy, D., Maroncelli, M., (2010), An Improved Four-Site Ionic Liquid Model. *The Journal of Physical Chemistry B*, *114*(39), 12629-12631.